

Crystal Field Analysis, Electron-phonon Coupling and Spectral Band Shape Modeling in MgO:Cr³⁺

Mikhail G. Brik

Fukui Institute for Fundamental Chemistry, Kyoto University, 34-4 Takano Nishihiraki-cho, Sakyo-ku, Kyoto 606-8103, Japan

Reprint requests to Dr. M. G. B.; E-mail: brik@fukui.kyoto-u.ac.jp

Z. Naturforsch. **60a**, 437–443 (2005); received August 4, 2004

A crystal field analysis of the energy level structure of Cr³⁺ in MgO crystal is performed, using the exchange charge model of the crystal field theory. The crystal field parameters acting on the optical electrons of Cr³⁺ are calculated from the crystal structure data; good agreement between the calculated and observed energy levels of Cr³⁺ in the title host is demonstrated. The Stokes shift $S = 5.9$ and the energy of the phonons effectively interacting with the impurity center $\hbar\omega = 405 \text{ cm}^{-1}$ are derived from the experimental spectra of absorption and emission. The obtained values of S and $\hbar\omega$ were used for the computer modeling of the Cr³⁺ ${}^4\text{T}_{2g} \rightarrow {}^4\text{A}_{2g}$ emission and ${}^4\text{A}_{2g} \rightarrow {}^4\text{T}_{2g}$ absorption bands. From this modeling, the zero-phonon energy for the considered transitions was estimated to be $14,000 \text{ cm}^{-1}$.

Key words: Crystal Field Theory; 3d-Ions; Electron-phonon Coupling.

1. Introduction

Trivalent chromium is a very important ion for solid state laser application. The crystals doped with Cr³⁺ have received considerable attention of researchers since 1960, when the first laser at all was realized with Al₂O₃:Cr³⁺ (ruby) [1]. Later on, many other crystals were shown to lase with the Cr³⁺ ion; the number of them now is about 20, and the lasers based on these hosts cover the spectral region between 700 nm and 1100 nm [2]. Such a wide tunability region is entirely due to the vibronic interaction between optical electrons of the Cr³⁺ ion and vibrations of the host lattice ions. Cr³⁺ is nearly always found in octahedral coordination, and in first approximation its energy level scheme can be described by the Tanabe-Sugano diagram for a cubic crystal field [3]. In most laser crystals there is a significant lowering of the local symmetry around an impurity ion due to the deformations of the crystal lattice. MgO exhibits specific properties with respect to deformation around the Cr³⁺ ion. When Cr³⁺ substitutes for Mg²⁺, charge compensation is required in form of vacancies in some Mg²⁺ sites in order to keep the electrical neutrality of the crystal. As shown by the EPR measurements [4–6], a large fraction of the Cr³⁺ ions do not have charge compensating vacancies nearby and are in sites of perfect octahe-

dral symmetry. Cr³⁺ ions in MgO can also occupy the sites of orthorhombic and tetrahedrally distorted symmetry [7], which occur near Mg²⁺ vacancies, but in the present work we will consider only perfect octahedral sites.

In this paper we use the crystal field theory to analyze the energy level scheme of the octahedrally coordinated Cr³⁺ ion in the title host, deduce the parameters of the electron-phonon coupling from the experimental data found in the literature, and perform a computer modeling of the Cr³⁺ ${}^4\text{T}_{2g} \rightarrow {}^4\text{A}_{2g}$ emission and ${}^4\text{A}_{2g} \rightarrow {}^4\text{T}_{2g}$ absorption bands shapes.

2. Crystal Structure and Spectroscopy of MgO:Cr³⁺

Magnesium oxide, MgO, is a cubic crystal which belongs to the $Fm\bar{3}m$ space group (space group number 225) with the lattice constant $a = 4.214 \text{ \AA}$ [8]. The unit cell consists of four formula units. Each Mg²⁺ ion is surrounded by six O²⁻ ions, the Cartesian coordinates of which obtained using data from [8], are given in Table 1.

The experimental spectroscopic data on Cr³⁺-doped MgO can be found in [2, 7]. The shape of the experimental spectra is typical for octahedrally coordinated Cr³⁺ ions. The following energy level assign-

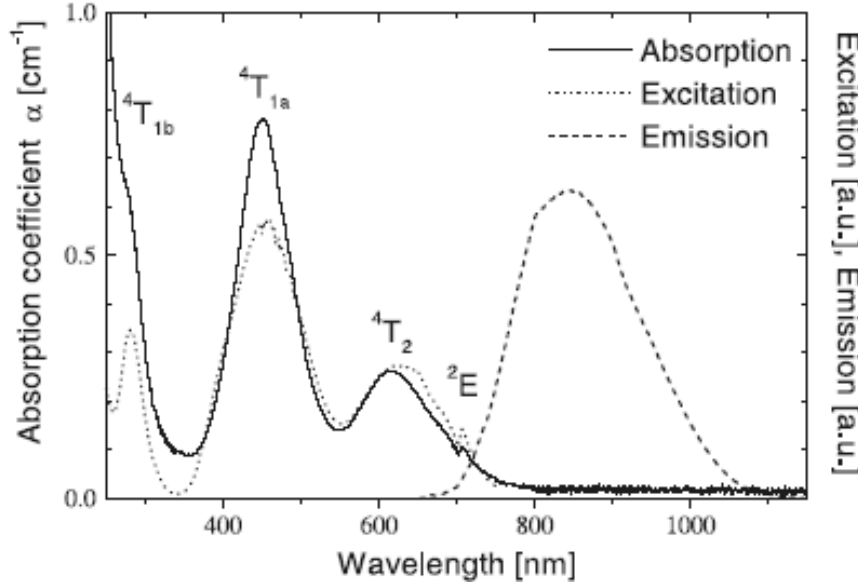


Fig.1. Absorption, excitation ($\lambda_{\text{em}} = 790$ nm), and emission ($\lambda_{\text{exc}} = 514$ nm) spectra of Cr-doped MgO at room temperature [2].

Table 1. Cartesian coordinates (in Å) of ions of the [CrO₆]⁹⁻ cluster in the MgO crystal.

Ion	<i>x</i>	<i>y</i>	<i>z</i>
Cr ³⁺	0	0	0
O ²⁻	2.107	0	0
O ²⁻	0	2.107	0
O ²⁻	0	0	2.107
O ²⁻	0	0	-2.107
O ²⁻	0	-2.107	0
O ²⁻	-2.107	0	0

ments (for the spin-allowed transitions) are given in [2]: ${}^4A_{2g}({}^4F) - {}^4T_{2g}({}^4F)$ at 619 nm (16,155 cm⁻¹), ${}^4A_{2g}({}^4F) - {}^4T_{1g}({}^4F)$ at 452 nm (22,124 cm⁻¹), ${}^4A_{2g}({}^4F) - {}^4T_{1g}({}^4P)$ at 283 nm (35,336 cm⁻¹). The sharp line around 706 nm (14,164 cm⁻¹) was assigned to the ${}^4A_{2g}({}^4F) - {}^2E_g({}^2G)$ spin-forbidden transition. The broad band emission between 700 and 1,050 nm, centered at around 850 nm was assigned to the ${}^4T_{2g}({}^4F) - {}^4A_{2g}({}^4F)$ transition of the Cr³⁺ ion. The crystal field strength *Dq* and Racah parameters *B* and *C* cited in [2] are (in cm⁻¹) 1,615, 586, and 3,249, respectively. Figure 1 shows the absorption, excitation ($\lambda_{\text{em}} = 790$ nm), and emission ($\lambda_{\text{exc}} = 514$ nm) spectra of Cr-doped MgO at room temperature [2].

3. Crystal Field Calculations for MgO:Cr³⁺

The energy levels of the Cr³⁺ ion in this work are represented by the eigenvalues of the crystal field

Hamiltonian of the form [9]

$$H = \sum_{p=2,4} \sum_{k=-p}^p B_p^k O_p^k, \quad (1)$$

where O_p^k are the linear combinations of irreducible tensor operators acting on the angular parts of the Cr³⁺ wave functions, and B_p^k are the crystal field parameters containing all information about the geometrical structure of an impurity center. As formulated in [9], these parameters can be written as a sum of two terms:

$$B_p^k = B_{p,q}^k + B_{p,s}^k. \quad (2)$$

The first contribution is due to the electrostatic interaction between optical electrons of an impurity ion and ions of the crystal lattice (treated as point charges, without taking into account their electron structure), and the second one is proportional to the overlap of the wave functions of an impurity ion and ligands. In other words, this term includes all effects of the covalent bond formation and exchange interaction. Inclusion of these effects significantly improves the agreement between the calculated and experimentally observed energy levels. Expressions for calculating both contributions to the crystal field parameters in the case of a 3d-ion are as follows [9]:

$$B_{p,q}^k = -K_p^k e^2 \langle r^p \rangle \sum_i q_i \frac{V_p^k(\theta(i), \varphi(i))}{R(i)^{p+1}}, \quad (3)$$

$$B_{p,s}^k = K_p^k e^2 \frac{2(2p+1)}{5} \sum_i \left[G_s S_s(i)^2 + G_\sigma S_\sigma(i)^2 + \gamma_p G_\pi S_\pi(i)^2 \right] \frac{V_p^k(\theta(i), \varphi(i))}{R(i)}. \quad (4)$$

The sums are carried out over lattice ions denoted by i with charges q_i ; $R(i)$, $\theta(i)$, $\varphi(i)$ are the spherical coordinates of the i -th ion of the crystal lattice in the reference system centered at the impurity ion. The averaged values $\langle r^p \rangle$ of p -th power of the impurity ion electrons radial coordinate can be found in [10]. The values of the numerical factors K_p^k , γ_p and expressions for the polynomials V_p^k are given in [9]. The overlap integrals between the d -functions of the central ion and the p - and s -functions of the ligands are denoted by S_s , S_σ , S_π [they correspond to the following integrals (in $\langle m|l'm' \rangle$ notation): $S_s = \langle d0|s0 \rangle$, $S_\sigma = \langle d0|p0 \rangle$, $S_\pi = \langle d1|p1 \rangle$]. G_s , G_σ , G_π are dimensionless adjustable parameters of the model, which are determined from the positions of the first three absorption bands. Very often they can be assumed to be equal to each other: $G_s = G_\sigma = G_\pi = G$ (in this case, only the first absorption band is required to determine the value of G). In this paper we use this simplified model. The advantage of the exchange charge model is that, if the G parameter is determined to fit the first absorption band, the other energy levels, located higher in energy, will also fit experimental spectra fairly well.

Initially the exchange charge model has been formulated and developed for rare earth ions [9], but later on it has been successfully applied to the transition metal ions in different hosts as well [11–15].

Since the second rank point charges parameters $B_{2,q}^k$ decrease not so fast as the fourth rank parameters $B_{4,q}^k$ (as $1/R^3$ and $1/R^5$, respectively), the contribution of the ligands from the second and further coordination spheres can be quite significant. To increase the accuracy in calculating the point charge contribution to the crystal field parameters, we considered a large cluster, consisting of 751 ions, namely, one ion of Cr³⁺, 380 ions of Mg²⁺, and 370 ions of O²⁻. This cluster enables to take into account the contribution of ions located at distances up to 11.919 Å. For the exchange charge parameters in (4) only the nearest ligands were taken into account, since the overlap between an impurity ion and ligands from other than the first coordination sphere can be safely neglected.

Using (1)–(4), the ligands positions from Table 1, and the Gaussian radial wave functions for the Cr³⁺

Table 2. Crystal field parameters (in cm⁻¹) of octahedral Cr³⁺ in MgO.

Parameter	Point charges contribution	Exchange charges contribution	Total value
B_4^0	841	3,400	4,241
B_4^4	4,204	17,000	21,204

Table 3. Positions of energy levels (in cm⁻¹) of octahedral Cr³⁺ in MgO.

O_h irrep. repres.	Experimental values [2]	Calculated (this work)
${}^4A_{2g}({}^4F)$	0	0
${}^4T_{2g}({}^4F)$	16,155	16,155
${}^4T_{1g}({}^4F)$	22,124	22,150
${}^4T_{1g}({}^4P)$	35,336	35,105

and O²⁻ ions from [16], we obtained the values of the non-zero crystal field parameters given in Table 2. To emphasize the role of the second term in (2) we give separately the values of the point charges and exchange charges parameters, and it is seen that the former are about 25% only from the latter.

The crystal field Hamiltonian was diagonalized in the space of 10 wave functions of the lowest 4F and 4P terms of the Cr³⁺ ion. The Racah parameter B , which defines the energy gap between the two above terms, was chosen to be 586 cm⁻¹ [2]. Significant reduction of this parameter in comparison to that for a free ion $\beta = B_{\text{complex ion}}/B_{\text{free ion}} = 0.64$ (for the free Cr³⁺ ion we use the value $B = 918$ cm⁻¹ [17]), known as the nephelauxetic effect is caused by the covalency. The strong nephelauxetic effect for Cr³⁺ in MgO indicates a high degree of covalency and serves as a firm justification of application of the exchange charge model for the considered case. The adjustable parameter G was defined by fitting the calculated splittings to the experimental ones, and turned out to be 15.005. The obtained energy levels are listed in Table 3, in comparison with experimental measurements.

4. Evaluation of the Parameters of Electron-phonon Interaction

To study the electron-phonon coupling of the Cr³⁺ ions with the lattice vibrations in MgO we used the single-coordinate configurational model in harmonic approximation [18]. This model is based on the assumption that the nearest environment of the impurity ion oscillates harmonically about its equilibrium position. This displacement is described by the Q coord-

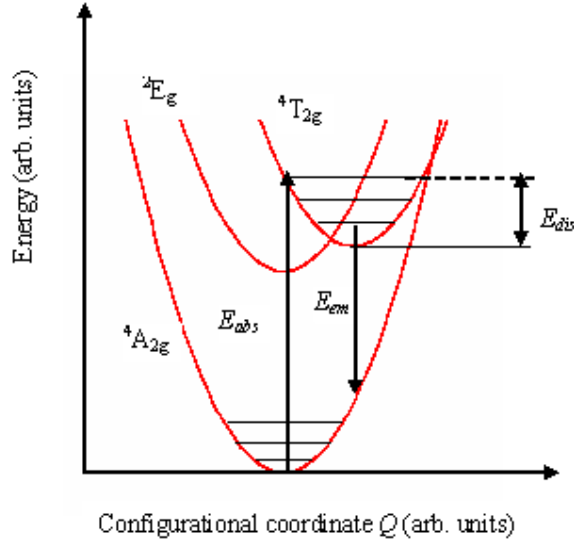


Fig. 2. Single-coordinate configurational diagram for MgO:Cr³⁺ (schematic representation). The lowest electronic states are shown; the vibrational frequencies in all electronic states are assumed to be the same. Vibrational energy levels are indicated by horizontal lines. Absorption and emission transitions are indicated by the up-ward and down-ward arrows, respectively. The difference between the excited state vibrational levels reached in the absorption transition and the minimum of the same parabola is denoted by E_{dis} .

dinate. A typical diagram of the potential energies of electronic states as a function of the vibrational coordinate Q for the case of a strong crystal field (when the orbital doublet 2E is located below the orbital triplet ${}^4T_{2g}$) is sketched in Figure 2.

The two main parameters which describe the electron-phonon coupling are the Huang-Rhys parameter S and the effective phonon energy $\hbar\omega$. The former is defined as the number of phonons of the energy $\hbar\omega$ excited in the absorption transition [18]:

$$S = \frac{E_{dis}}{\hbar\omega}, \quad (5)$$

where E_{dis} is defined in Figure 2. S and $\hbar\omega$ are related to the difference between the first absorption and corresponding emission band peaks ΔE by the expression [18, 19]:

$$\Delta E = (2S - 1)\hbar\omega. \quad (6)$$

The second equation which is required to calculate the values of S and $\hbar\omega$ is [18]

$$\Gamma(T) = 2.35\hbar\omega \sqrt{S \coth\left(\frac{\hbar\omega}{2kT}\right)}, \quad (7)$$

where $\Gamma(T)$ is the emission band full width at half maximum (FWHM) at the absolute temperature T . In order to solve (6) and (7) we used the spectroscopic data from [2]. According to these data, the energetical Stokes shift ΔE is about $4,377 \text{ cm}^{-1}$, and the FWHM of the ${}^4T_{2g} \rightarrow {}^4A_{2g}$ emission band at 300 K is about $2,654 \text{ cm}^{-1}$. Solving (6) and (7) yields $S = 5.9$, $\hbar\omega = 405 \text{ cm}^{-1}$. It is interesting to compare the obtained value of the effective phonon energy $\hbar\omega$ with the results for the fluoride crystals ($\hbar\omega = 260 \text{ cm}^{-1}$ for Cs₂NaAlF₆:Cr³⁺ [19]). The energy of the effective phonon in MgO is 1.6 times larger than in the fluoride. Therefore, a smaller number of phonons would be required to bridge the ${}^4T_{2g} - {}^4A_{2g}$ energy gap and non-radiative quenching of the ${}^4T_{2g}$ state in MgO would be more probable than in fluorides. This conclusion is supported by the experimental measurements of the ${}^4T_{2g} - {}^4A_{2g}$ emission lifetime reported in [2] for MgO:Cr³⁺ (it is about $30 \mu\text{s}$ at 300 K) and in [20] for Cs₂NaAlF₆:Cr³⁺ (it is significantly greater, about $180 \mu\text{s}$ at 300 K, indicating the less important role of the non-radiative processes in quenching of the excitation energy in the last case).

5. Computer Modeling of the ${}^4T_{2g} \rightarrow {}^4A_{2g}$ Emission and ${}^4A_{2g} \rightarrow {}^4T_{2g}$ Absorption Bands Shapes in MgO:Cr³⁺

Since the electron-phonon interaction affects significantly the absorption and emission processes taking place at the impurity center, the modeling of the emission and absorption bands can serve as a reliable test for the validity of that obtained in the previous section for parameters of the electron-phonon coupling. Again, the single configuration coordinate model can be employed. In the framework of this model, the emission and absorption band shapes are given by the expression [18]

$$I = I_0 \sum_m \exp(-S) \frac{S^m}{m!} \delta(E_0 \mp m\hbar\omega - E), \quad (8)$$

where I is the intensity of the band, E_0 the zero-phonon energy, E the photon energy, m an integer (this is the number of phonons involved in the transition) and all other quantities entering (8) are defined above. The “-” sign relates to the emission transition, and the “+” sign to the absorption transition. The only parameter which has not been defined yet and which is allowed to vary freely is E_0 . The best fit of the experimental and calculated band shapes was obtained for $E_0 = 14,000 \text{ cm}^{-1}$.

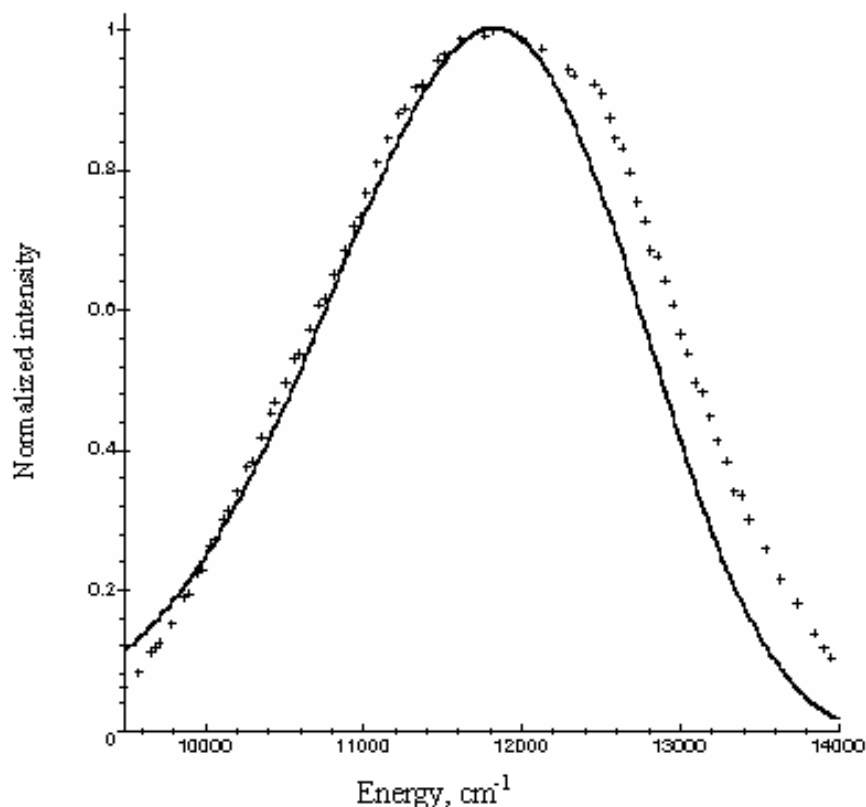


Fig. 3. Theoretical (solid line) and experimental (crosses, [2]) band shapes of the ${}^4T_{2g} \rightarrow {}^4A_{2g}$ emission transition in MgO:Cr³⁺.

The results of the calculations are shown in Fig. 3 (for the emission band) and Fig. 4 (for the absorption band), respectively.

The experimental band shapes (which are shown by crosses in both figures) have been obtained by scanning the corresponding curves from Fig. 1 and recalculating the wavelengths into the wavenumber scale; the theoretical curves are shown by the solid lines. Both experimental and theoretical band shapes have been normalized to unity, for easiness of comparison. As can be seen from Figs. 3 and 4, the maximum positions of the experimental and theoretical curves coincide. The shape of the calculated ${}^4T_{2g} \rightarrow {}^4A_{2g}$ emission band agrees pretty well with the experimental one (the last one is just a bit wider). In the case of the ${}^4A_{2g} \rightarrow {}^4T_{2g}$ absorption band the shape agreement is a bit worse, but one has to keep in mind an overlap between this transition and the ${}^4A_{2g} \rightarrow {}^2E_g$ (around 14,100 cm⁻¹) and ${}^4A_{2g} \rightarrow {}^4T_{1g}$ (at 18,000 cm⁻¹ and above) transitions, which is clearly seen in experimental spectra (Fig. 1) and which can not be taken into account by (8). One additional reason for the experimental bands to be broader than the calculated ones should be also pointed

out: the single configuration coordinate model considers the interaction of the impurity ion with one normal mode of vibration only, whereas the experimental spectra are the result of the complicated interaction between several vibrational modes and the impurity ion.

6. Conclusions

Calculations of the crystal field parameters and energy level structure of the octahedrally coordinated Cr³⁺ ion in MgO were performed in the framework of the exchange charge model of the crystal field, which has only one adjustable parameter G , describing the overlap between the wave functions of the central ion and its ligands. A good agreement between the calculated and observed energy levels of the Cr³⁺ ion in MgO was obtained. The exchange charge model with its possibility of explicit inclusion of the overlap integrals into the expression for calculating the crystal field parameters provides an adequate description of the energy levels scheme of Cr³⁺ in the studied crystal. The Stokes shift $S = 5.9$ and the effective phonon energy $\hbar\omega = 405$ cm⁻¹ have been deduced

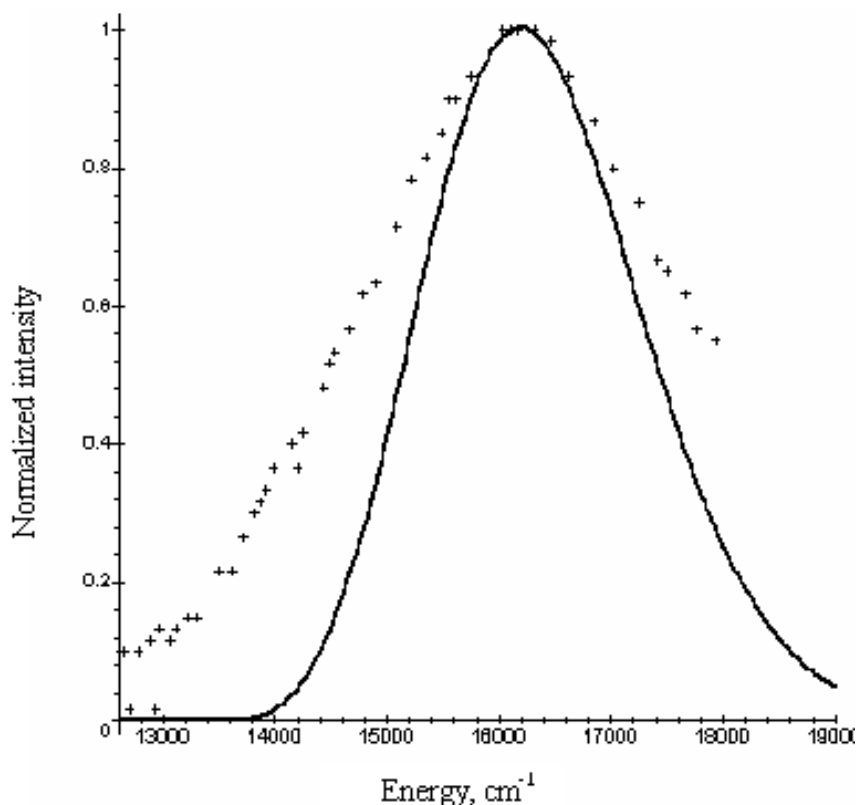


Fig. 4. Theoretical (solid line) and experimental (crosses, [2]) band shapes of the ${}^4A_{2g} \rightarrow {}^4T_{2g}$ absorption transition in MgO:Cr³⁺.

from the experimental spectra of emission and absorption of MgO:Cr³⁺. The Cr³⁺ ${}^4T_{2g} \rightarrow {}^4A_{2g}$ emission and ${}^4A_{2g} \rightarrow {}^4T_{2g}$ absorption band shapes were calculated using the single configuration coordinate model. Fitting of the calculated band shapes to the experimental spectra allowed for estimating the zero-phonon energy of the considered transitions to be 14,000 cm⁻¹.

Acknowledgements

Financial support from the Japanese Ministry of Education, Culture, Sports, Science and Technology (MEXT) in a project on computational materials science unit at Kyoto University is gratefully acknowledged.

- [1] T. H. Maiman, *Nature London* **187**, 493 (1960).
- [2] S. Kuck, *Appl. Phys. B* **72**, 515 (2001).
- [3] S. Sugano, Y. Tanabe, and H. Kamimura, *Multiplets of Transition-metal Ions in Crystals*, Academic Press, New York 1970.
- [4] J. E. Wertz and P. Auzins, *Phys. Rev.* **106**, 484 (1957).
- [5] J. H. E. Griffiths and J. W. Orton, *Proc. Phys. Soc. London* **73**, 948 (1959).
- [6] B. Henderson and J. E. Wertz, *Adv. Phys.* **17**, 749 (1968).
- [7] M. O. Henry, J. P. Larkin, and G. F. Imbush, *Phys. Rev. B* **13**, 1893 (1976).
- [8] V. G. Tsirel'son, A. S. Avilov, Yu. A. Abramov, E. L. Belokoneva, R. Kitaneh, and D. Feil, *Acta Crystallogr. B* **54**, 8 (1998).
- [9] B. Z. Malkin, Crystal field and electron-phonon interaction in rare-earth ionic paramagnets, in: *Spectroscopy of Solids Containing Rare-earth Ions* (Eds. A. A. Kaplyanskii, B. M. Macfarlane), North-Holland, Amsterdam 1987, pp. 33–50.
- [10] A. G. Abragam and B. Bleaney, *Electron Paramagnetic Resonance of Transition Ions*, Clarendon, Oxford 1970, chapter 7.
- [11] A. G. Avanesov, V. V. Zhorin, B. Z. Malkin, and V. F. Pisarenko, *Sov. Phys. Solid State* **34**, 1552 (1992).
- [12] M. G. Brik, C. N. Avram, and N. M. Avram, *OSA Trends in Optics and Photonics*, in: *Advanced Solid-state Lasers*, Vol. **68** (Eds. M. E. Fermann and L. R. Marshall), Optical Society of America, Washington, DC 2002, pp. 275–279.

- [13] M. G. Brik and C. N. Avram, *J. Lumin.* **102–103**, 283 (2003).
- [14] C. Jousseume, D. Vivien, A. Kahn-Harari, and B. Z. Malkin, *Opt. Mater.* **24**, 143 (2003).
- [15] M. G. Brik, C. N. Avram, and I. Tanaka, *Phys. Status Solidi (b)* **241**, 2501 (2004), DOI 10.1002/pssb.200402041.
- [16] M. V. Eremin, in: *Spectroscopy of Crystals*, Nauka, Moscow 1989, pp. 30–44 (in Russian).
- [17] R. C. Powell, *Physics of Solid-state Laser Materials*, Springer, Berlin 1998.
- [18] B. Henderson and G. F. Imbush, *Optical Spectroscopy of Inorganic Solids*, Clarendon Press, Oxford 1989.
- [19] G. A. Torchia, O. Martinez-Matos, N. M. Khaidukov, and J. O. Tocho, *Solid State Commun.* **130**, 159 (2004).
- [20] L. P. Sosman, A. D. Tavares Jr., R. J. M. da Fonseca, T. Abritta, and N. M. Khaidukov, *Solid State Commun.* **114**, 661 (2000).